



3D QSAR (COMFA) of a series of potent and highly selective VLA-4 antagonists

Juswinder Singh^a, Herman van Vlijmen^a, Wen-Cherng Lee^a, Yusheng Liao^a, Ko-Chung Lin^a, Humayun Ateeq^a, Julio Cuervo^a, Craig Zimmerman^a, Charles Hammond^a, Michael Karpusas^a, Rex Palmer^b, Tapan Chattopadhyay^b & Steven P. Adams^a

^a*Biogen Inc, 12 Cambridge Center, Cambridge MA02142, USA*

^b*Dept. of Crystallography, Birkbeck College, University of London, Malet Street, London, WC1E 7HX, U.K.*

Received 4 December 2001; Accepted 30 April 2002

Key words: 3D-QSAR, COMFA, VCAM-1, VLA-4

Summary

The integrin VLA-4 ($\alpha 4\beta 1$) is involved in the migration of white blood cells to sites of inflammation, and is implicated in the pathology of a variety of diseases including asthma and multiple sclerosis. We report the structure-activity relationships of a series of VLA-4 antagonists that were based upon the integrin-binding sequence of the connecting segment peptide of fibronectin (Leu-Asp-Val), and of VCAM-1 (Ile-Asp-Ser), both natural ligands of VLA-4. We explore variation in the ligand derived peptide portion of these antagonists and also in the novel N-terminal cap, which have discovered through chemical optimization, and which confers high affinity and selectivity. Using the X-ray derived conformation of the Ile-Asp-Ser region of VCAM-1, we rationalize the structure-activity relationships of these antagonists using 3D QSAR (COMFA). The COMFA model was found to be highly predictive with a cross-validated R^2_{CV} of 0.7 and a PRESS of 0.49. The robustness of the model was confirmed by testing the influence of various parameters, including grid size, column filtering, as well as the role of orientation of the aligned molecules. Our results suggest that the VCAM-1 structure is useful in generating highly predictive models of our VLA-4 antagonists. The COMFA model coupled with the knowledge that the peptide amides are tolerant to methylation should prove useful in future peptidomimetic design studies.

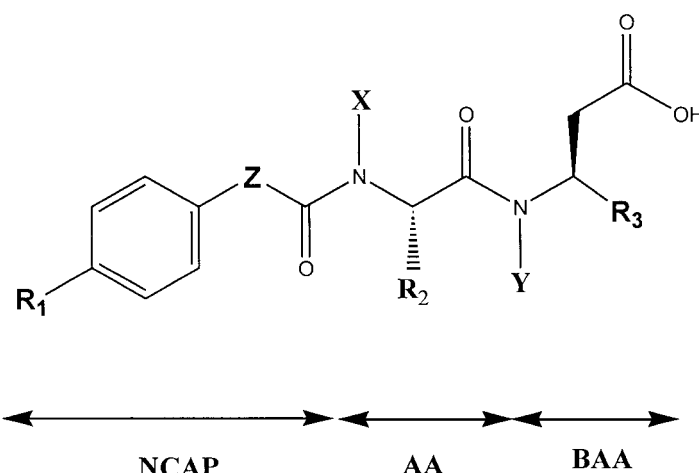
Introduction

The integrin VLA-4 ($\alpha 4\beta 1$) is a heterodimeric receptor involved in cell-cell and cell-extracellular matrix adhesion. VLA-4 is known to bind the alternatively-spliced type-III connecting-segment of fibronectin in the extracellular matrix and vascular cell adhesion molecule-1 (VCAM-1) expressed on activated endothelium. Due to its role in the inflammatory response, VLA4 is an attractive target for therapeutic intervention. The involvement of VLA4 in disease has been studied using anti-VLA-4 monoclonal antibodies [1], CS-1 peptides from fibronectin [2] and small molecule antagonists of $\alpha 4\beta 1$ [3]. These studies confirm that $\alpha 4$ integrin dependent adhesion pathways are critical intervention points in several models of inflammatory and autoim-

mune pathologies, including asthma [4, 5], ulcerative colitis [6], diabetes [7, 8], multiple sclerosis [1, 9] and arthritis [10].

The site of fibronectin binding to VLA-4 has been studied through peptide mapping studies by Komoriya et al. [11] who identified Leu-Asp-Val as the minimum sequence for cell adhesion. This sequence is similar to the Ile-Asp-Ser region of VCAM-1, which has been identified as the integrin binding region [12]. Makarewicz et al. [13] have shown that VCAM-1 and fibronectin can compete for binding to VLA-4, which suggests that the Ile-Asp-Ser region of VCAM-1 and Leu-Asp-Val region of fibronectin bind either identical or overlapping sites on the receptor.

The sequences and structures of these integrin-binding motifs have been employed as starting points



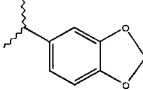
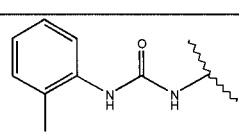
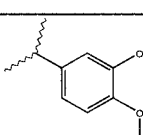
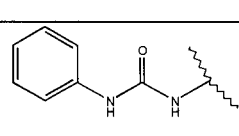
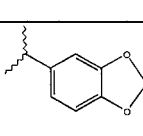
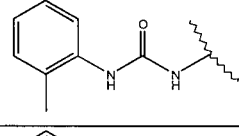
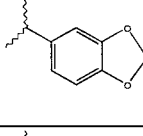
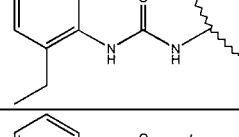
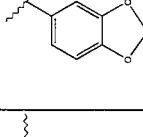
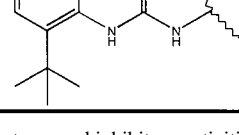
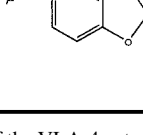
#	R ₁	R ₂	R ₃	Z	X	Y	IC ₅₀ (nM)
1	OH	Leu		CH ₂	H	H	153
2		Leu		N	H	H	3
3		Leu		CH ₂	H	H	12
4		Leu		CH ₂	H	H	1.5
5		Leu		CH ₂	H	H	214
6		Leu		CH ₂	H	H	662

Figure 1. Chemical structures and inhibitory activities (IC₅₀s) of the VLA-4 antagonists. The IC₅₀ data were calculated from inhibition curves resulting from the concentration-dependent inhibition of VCAM-Ig binding to VLA-4.

#	R ₁	R ₂	R ₃	Z	X	Y	IC ₅₀ (nM)
7		Leu		CH ₂	H	H	535
8		Leu		CH ₂	H	H	200
9		Leu		CH ₂	H	H	3
10		Leu		CH ₂	H	H	60
11		Leu		CH ₂	H	H	3
12		Leu		CH ₂	H	H	3.5
13		Leu		CH ₂	H	H	10
14		Leu		CH ₂	H	H	21
15		Leu		CH ₂	H	H	90

Figure 1. Continued.

#	R ₁	R ₂	R ₃	Z	X	Y	IC ₅₀ (nM)
16		Leu		CH ₂	H	H	35
17	CF ₃ 	Leu		CH ₂	H	H	56
18		Pro		CH ₂	-	H	30
19		Pro	CH ₃	CH ₂	-	H	7.5
20		Pro		CH ₂	-	H	5.5
21		Met		CH ₂	H	H	1.5

Figure 1. Continued.

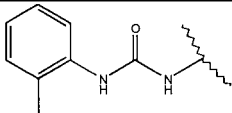
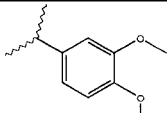
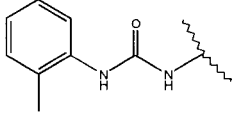
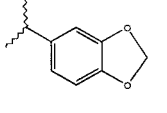
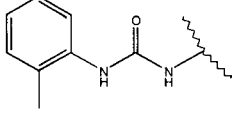
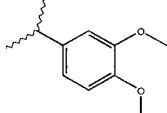
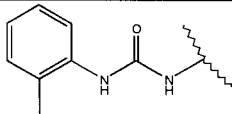
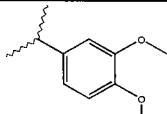
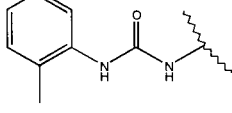
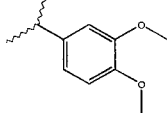
#	R ₁	R ₂	R ₃	Z	X	Y	IC ₅₀ (nM)
25		Leu		CH ₂	CH ₃	H	1
26		Pro		CH ₂	-	H	7
27		Ala		CH ₂	CH ₃	H	8
28		Met		CH ₂	CH ₃	H	2
29		Lys		CH ₂	H	H	2.5

Figure 1. Continued.

in the design of small molecule antagonists of $\alpha 4\beta 1$. The crystal structure of domains 1 and 2 of VCAM-1 reveals that the Ile-Asp-Ser integrin binding region occurs on a highly exposed loop [14, 15] with well defined structure. The crystal structure of MadCAM, another ligand for $\alpha 4$ integrins, has also been determined, and although the sequence of the integrin binding site is different (Leu-Asp-Thr), it has a similar local conformation to that in VCAM-1. At present, there is no structure of CS1, but the sequence similarity (Leu-Asp-Val) suggests they may adopt a similar conformation. Recently, a Leu-Asp-Val based inhibitor (Bio1494), based upon a series of subnanomolar inhibitors selective for $\alpha 4\beta 1$ and its ligands, was described [16].

Currently, there is no detailed structural information available on the VLA-4 receptor. One approach to gain structural insight into the binding site is to compare the structure-activity data of a series of molecules that bind to the receptor [17]. Using Comparative

Molecular Field Analysis (COMFA; [18]) it is possible to derive a 3-dimensional quantitative structure-activity relationship (3D QSAR) for inhibitors. The method requires as input a structural alignment of compounds in their presumed binding mode together with their biological activities. Molecular fields (electrostatic and steric) surrounding each molecule are then calculated using probes located at points on a lattice that encompass the molecule. A partial least squares analysis of the biological activities and molecular fields of each molecule allows a QSAR to be derived. The steric and electrostatic fields in the model can then be visualized in 3D to provide a prediction of the receptor binding site requirements.

To our knowledge, there has been no QSAR analysis reported for inhibitors of VLA-4; thus, we have employed the crystal structure of VCAM-1 to build a 3D QSAR model for a series of structurally-related VLA4 inhibitors. The inhibitors were based on a novel capped-peptide strategy typified by the compound 4-

[N'-(2-methylphenyl)ureido]phenylacetyl-LDVP [19]. Our results suggest that the VCAM-1 structure is useful in generating highly predictive models of our VLA-4 antagonists.

Materials and methods

Model building

A 3D model for each of the 29 compounds (Figure 1) was constructed using the BUILDER module within InsightII (version 95.0, Biosym Technologies). All energy calculations were performed using the CVFF forcefield within DISCOVER and the potentials were set for each of the compounds using the ForceField/Potential command.

The compounds have the general formula NCAP-AA-BAA (Figure 1), in which NCAP is an amino terminal cap, AA is a natural amino acid (Leu, Met, Pro and Lys) and BAA is a β -amino acid. The approach used to build the compounds models is illustrated with **4**. The side chain and main chain torsion angles for the AA-BAA section of compound **4** were built using corresponding values from the Ile39-Asp40 region of VCAM-1 ([14]; protein database code: 1VCA). The β -amino acid side chain (phenylmethylenedioxy) and the NCAP portion (4-[N'-(2-methylphenyl)ureido]phenylacetyl) were then attached to the AA-BAA fragment. The NCAP and BAA side chains were energy minimized using 1000 steps of steepest descent while the rest of the structure was held fixed. Using a systematic conformational search the lowest energy conformation of the BAA and NCAP side chains were identified. The systematic conformational search employed the Search/Compare module of InsightII, using the default settings with a 30 degree step size and the ENERGY option set to on. During the minimization all corresponding torsions derived from the Ile39-Asp40 region of VCAM-1 were held fixed. After each step in the conformational search the BAA side chain and NCAP were subjected to 500 steps of energy minimization using the Optimize option (default parameters), and the lowest energy conformation was selected.

COMFA setup

The conformational models were input into COMFA as implemented in Sybyl 6.3 (Tripos Associates, 1699 S. Hanley Road, Suite 303, St. Louis, MO 63144). The

biological activities were expressed as $-\log(\text{IC}_{50})$. The default COMFA parameters were used.

In order to assess the predictive value of our models, we used cross-validation to determine the predictive r^2 (R_{CV}^2). The R_{CV}^2 was as defined by Cramer [18].

To explore the influence of the orientation of the aligned molecules on the predictivity of the COMFA model, we systematically rotated the aggregate of aligned molecules around the x, y and z axes in 30° increments using the Sybyl STATIC command.

Guided-region selection COMFA analysis (GRS)

The GRS analysis was performed as described by Cho and Tropsha ([20]), using a series of spl and awk scripts obtained from Dr. S. Cho; <http://mmlin1.pha.unc.edu/~jin/QSAR>). The number of components was set to 10, and the optimal number of components (ONC) was that with the highest cross-validated R-squared (R_{CV}^2).

Biological assay

The compounds were evaluated in a direct binding assay using a VCAM-Ig fusion protein as ligand, which has been reported in detail elsewhere [21].

X-ray Analysis of Compound 19

For crystal structure determination, **19** was crystallized from various solvents. Optically sound, approximately equidimensional, block-shaped crystals were obtained after a few days. The crystal system was monoclinic and the space group was $P2_1$. The unit cell dimensions were $a = 13.759 \text{ \AA}$, $b = 9.299 \text{ \AA}$, $c = 19.63 \text{ \AA}$, $\alpha = 90^\circ$, $\beta = 97.56^\circ$ and $\gamma = 90^\circ$. The quality of the diffraction was shown to be low from Oscillation and Weissenberg photographs and Mar Image Plate images using Cu radiation.

Because of the low quality of the diffraction of data from the first crystal, data collection at low temperature was undertaken. A new crystal was mounted on a Bruker SMART CCD X-ray system using with $M_o K_\alpha$ radiation and a full set of data was recorded at 173°K. These low temperature measurements served the intended purpose by improving the relative intensity of the X-ray reflections due to decrease of the crystallographic thermal displacement parameters and eliminating much of the static disorder suspected to be present at room temperature. Even at low temperature the diffraction quality was not very good and required

long exposures. Some residual disorder was found in molecule B which was thought to influence the quality of the data. Despite these deficiencies an accurate structure was derived and refined from this crystal. A total of 14851 X-ray reflections were processed.

The structure was determined using the direct methods algorithms in the SHELX package (<http://shelx.uni-ac.gwdg.de/SHELX/>). With two independent molecules, A and B per asymmetric unit, the analysis required determination of 70 non-H atoms. Non-H atoms were assigned with reference to the molecular geometry. Following isotropic and then anisotropic refinement of the non-H atoms fragment, H-atoms were calculated using geometrical methods. H-atoms were subsequently included in the refinement and with group isotropic thermal displacement parameters. Assignment of heavy atoms and inclusion of H atoms have been made throughout to be consistent with the geometry of their bonding environment.

Results and discussion

Figure 1 lists the 2D structures and receptor affinities of the VLA-4 antagonists used in the analysis. The compounds were evaluated in a direct binding assay in which IC₅₀ data were calculated from inhibition curves resulting from the concentration-dependent inhibition of VCAM-Ig binding to VLA-4 [21]. The compounds were defined in three parts (NCAP, AA and BAA). The AA group explored variation in charged and hydrophobic amino acids, and exhibited a preference for longer side chains, with an up to 8-fold increase in potency for Leu (**25**, IC₅₀ 1 nM) over Ala (**27**, IC₅₀ 8 nM) and Pro (**26**; IC₅₀ 7 nM). The BAA portion explored a variety of β -amino acids, and appeared to be generally tolerant to substitution, including large aromatic groups (**4**, IC₅₀ 1.5 nM). The least favored substitution, involved a carboxyl group (**18**, IC₅₀ 30 nM; **20**, IC₅₀ 5.5 nM), which may be a consequence of unfavorable electrostatic repulsion between the two β -amino acid carboxyls. It is notable that methylation of the AA and BAA peptide units was tolerated, which suggests these positions may be amenable to peptidomimetic strategies. The methylation of the AA amide resulted in a modest increase in activity (**2**, IC₅₀ 3 nM; **25**, IC₅₀ 1 nM), while the methylation of the β -amino acid amide unit resulted in a modest decrease in activity (**19**, IC₅₀ 7.5 nM; **22**, IC₅₀ 23 nM). The NCAP was discovered through chemical optimization. The most potent N-terminal

cap was the ortho-methyl phenylurea, which provided an additional 100-fold increase in potency (**1**, IC₅₀ 153 nM; **4**, IC₅₀ 1.5 nM). The urea amides appear to play a role in binding, with substitution of either of the nitrogens by oxygen resulting in a 7-fold (**3**, IC₅₀ 12 nM; **15**, IC₅₀ 90 nM) and 3-fold loss in activity (**3**, IC₅₀ 12 nM; **16**, IC₅₀ 35 nM) respectively. The ortho-position of the diphenylurea was sensitive to substitution, with bulky substituents resulting in significant loss (>400-fold) of inhibitory activity (**4**, IC₅₀ 1.5 nM; **6**, IC₅₀ 662 nM).

In order to understand the structural basis for inhibition, we built a 3D structural alignment of all the 29 compounds, using the crystal structure of the integrin-binding region of VCAM-1 as a template. The AA portion was based on the Ile39, and the BAA portion on the Asp 40 region of the integrin-binding motif of VCAM-1. The NCAP portion of the inhibitors was not based upon the VCAM-1 structure and was model-built using conformational search methods. The principal axes of the aligned compounds are 26 Å \times 12.9 Å \times 9.1 Å which provides an extensive surface area to bind the receptor. The majority of the chemical functionality on each of the compounds is highly exposed, and would be available for interaction with the VLA-4 binding site; however, intramolecular packing between the BAA and AA side chain is observed for some of the compounds. The diphenylurea accounts for a large fraction of the accessible surface of the compounds (56% of **3**). In the model, the phenyl rings of the diphenylurea portion are coplanar (interplanar angle 0°). We verified the coplanarity of the rings by analyzing the diphenylurea moieties present in the Cambridge Crystallographic Database [22], and by semi-empirical energy minimizations (MOPAC) [23]. Two alternative orientations of R1 are possible by 180° rotation around the R1-phenyl bond. We used the orientation as shown in Figure 1 for our calculations.

X-ray determination of 19

To complement conclusions about the conformational model developed for the series of VLA4 antagonists, a separate crystallographic study was undertaken on **19**. The X-ray crystal structure revealed two molecules of **19** (Structure 1 and Structure 2; Figure 2) in the asymmetric unit, coordinated through a network of hydrogen bonds mediated by two water molecules. The two molecules adopt essentially the same conformation, however there were differences in the ring

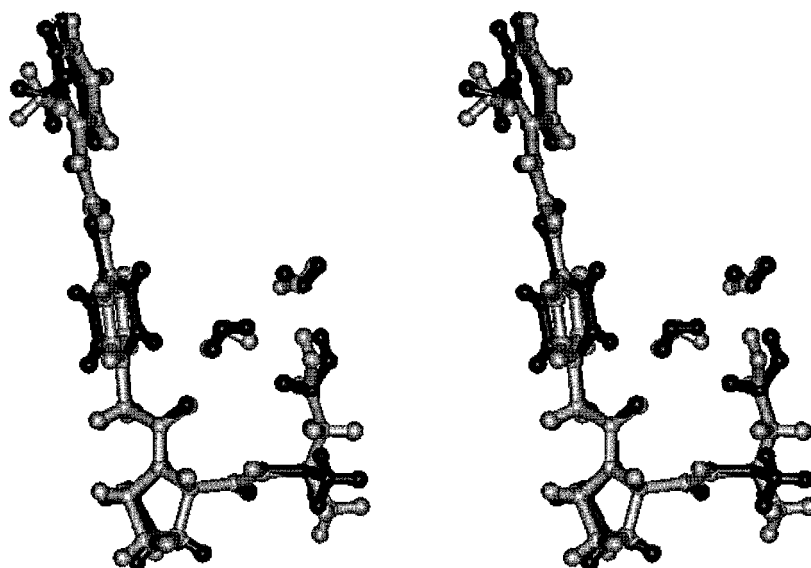


Figure 2. Stereo view of the overlay of the two molecules from the asymmetric unit of the X-ray structure of **19**.

puckering of the Pro side chain, and more significantly, in the conformation of the Pro-BAA peptide unit and the position of the BAA methyl side chain (Figure 2). This is also the sole region of disorder in the crystal structure. There were also differences in the water-mediated hydrogen-bond network. In Structure 1, one water molecule bridges the carbonyl oxygen of the phenylacetyl to the carboxyl of the BAA group while the second water molecule bridges between the other carboxyl oxygen and the first water molecule. In Structure 2, one water molecule bridges between the carbonyl oxygen of the phenylacetyl to the second water molecule. This second water molecule is also involved in an interaction with one of the carboxyl oxygens.

A comparison of the X-ray crystal structure to our model of **19** reveals a high degree of similarity (Figure 3). The major difference between them is the conformation of the Pro-BAA peptide unit and the BAA side chain methyl. This was also the major difference between the two molecules of the X-ray structure. The RMS deviation of the model with Structure 1, excluding the Pro-BAA peptide unit and BAA methyl, was 0.3 Å. The diphenylurea portion of the X-ray structure showed the phenyl rings were essentially coplanar with each other (interplanar angle $\sim 18^\circ$) and with the plane of the urea moiety (interplanar angle $\sim 14^\circ$) which was consistent with our prediction.

COMFA analysis

The initial COMFA on the 29 aligned compounds using a grid box of 2 Å resolution, showed the model to be highly predictive, with a R_{cv}^2 of 0.68 and a PRESS of 0.49. It has been suggested that R_{cv}^2 values greater than 0.3 are significant [24]. To assess the effect on R_{cv}^2 of a more finely sampled grid-box we set the grid spacing to 1 Å. It was found in this case that a 1 Å spacing resulted in a highly predictive model (Run 2), with a R_{cv}^2 of 0.7 and a PRESS of 0.49 (ONC=5). As a means to explore the influence of orientation of the aligned molecules on the predictivity of our model, we used the q^2 -GRS-routine [20] to generate an orientation independent COMFA model. This approach involves running COMFA separately on a lattice subdivided into 125 small boxes. The subset of 125 boxes with R_{cv}^2 above a threshold value, are retained for the final COMFA analysis. Our results show that using this method we also generate a highly predictive model with an R_{cv}^2 of 0.73 and PRESS of 0.4 (ONC=5). We also evaluated the COMFA model resulting from the alternative R1 orientation around the R1-phenyl bond and found a R_{cv}^2 of 0.54, indicating that the first orientation was more predictive.

To explore the effect of column filtering, we repeated our COMFA run, using the 1.0 Å grid spacing, this time without column filtering switched on (Run 3). The results were identical to that with column filtering switched on (Run 2). The contribution of steric and electrostatic field types to the model sug-

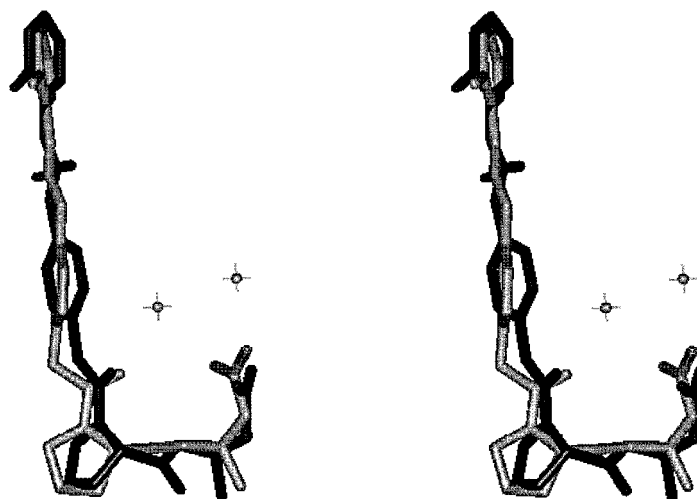


Figure 3. Stereo view of the overlay between the X-ray structure of **19** (Gray) and our model of **19** (Black).

gest that steric terms predominate (the mean ratio of electrostatic to sterics was 0.2/0.8).

In order to assess the likelihood that the high R_{CV}^2 we observed could of occurred by chance we performed 100 COMFA runs using scrambled biological data. The results shows a mean R_{CV}^2 of -0.18 with a standard deviation of 0.15.

COMFA fields

Using COMFA it is possible to visualize the QSAR fields in 3-dimensions by contouring the coefficients from the steric and electrostatic terms. In Figure 4 we have contoured the std*coeff fields of the electrostatic terms in the QSAR, to identify those regions in which the presence of positive potential would either be favorable to the biological activity (blue regions) or detrimental (red regions). There exists a large area directly in front of the urea nitrogens where positive potential is predicted to be favorable for binding, and an area nearby the carbonyl oxygen of the urea moiety where negative potential is favorable. Interestingly, the region of positive potential in our model is near Arg36 (4.7 Å; ureaNH–ArgNH₂) which has been shown through mutagenesis studies to be crucial for binding of VCAM-1 to VLA-4 [26]. Furthermore, the region of negative potential is near Glu81 (4.8 Å; ureaCO–Glu81OE2) which is also involved in binding of VCAM-1 to VLA-4 [25].

In Figure 4 we have contoured the std*coeff fields for the steric terms in the QSAR, to identify those regions where the presence of steric bulk would either

be favorable to the biological activity (green regions) or detrimental (yellow regions). The steric maps show density near the AA-BAA side chains. The intramolecular packing of the AA and BAA groups with each other creates a continuous hydrophobic patch on one face of the aligned compounds which would be available for interaction with a receptor. The steric contour map suggests strict steric requirements at the ortho-substituted ring of the diphenylurea. The map shows that steric bulk in the plane of the ring directly at the ortho position is favorable for binding (green density), but that steric bulk out of the plane is unfavorable (yellow density). One possible explanation for this is that the ring accesses a narrow slot on the receptor which has a requirement for planar substituents. Visual inspection of the VCAM-1 surface does not identify any obvious steric groups which could act as mimics of the hydrophobic portion of the N-terminal cap, which suggests that this may be a unique feature of these small molecule antagonists. Alternatively, a conformational change in VCAM upon binding to VLA4 could position VCAM functionality in an analogous orientation.

Conclusion

The development of VLA4 antagonists is an active area of drug discovery research within the pharmaceutical industry. We have described a possible structural basis for the receptor activity of a series of potent VLA-4 inhibitors. Although no atomic-level structural information is yet available for the VLA-4 receptor

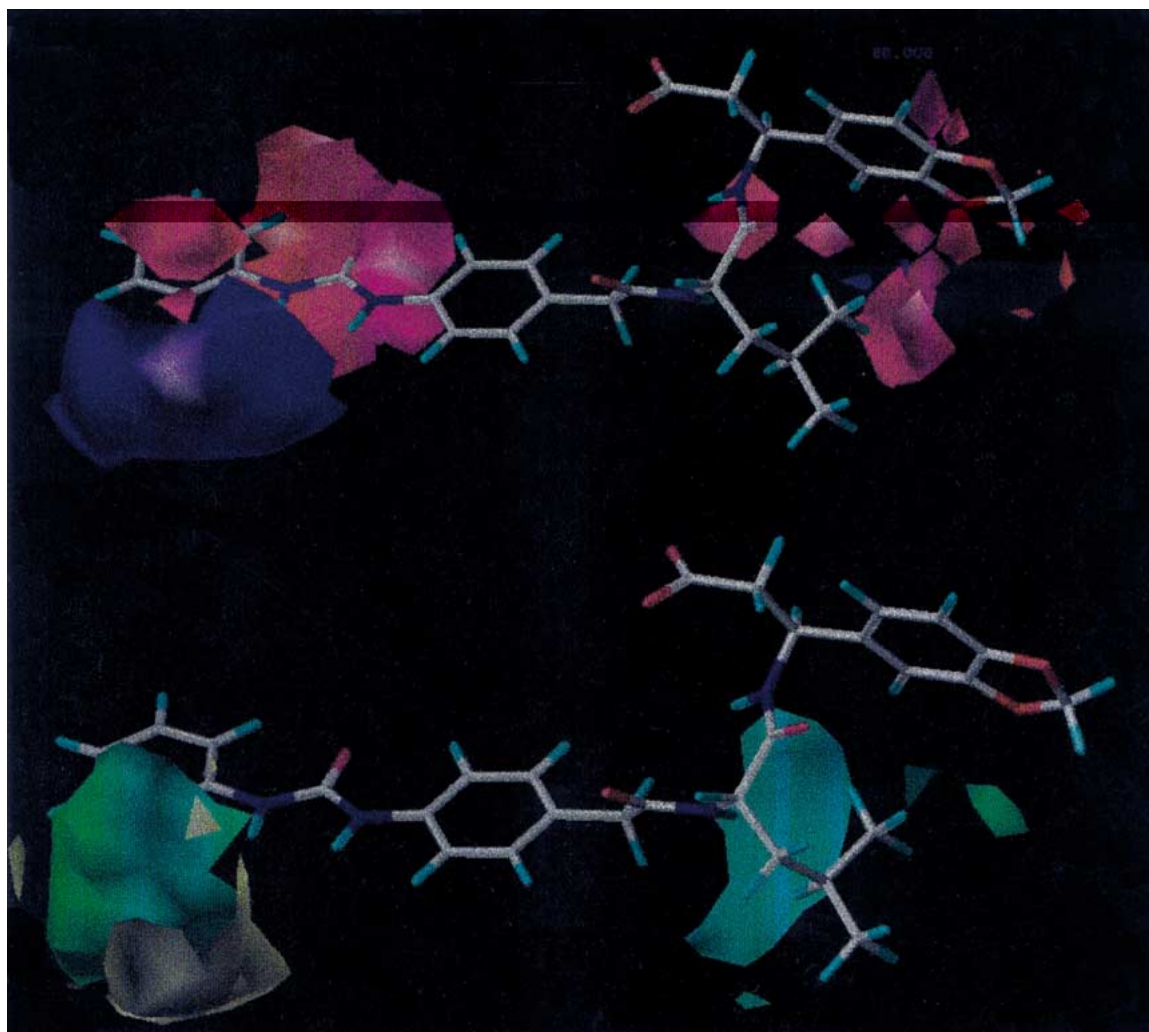


Figure 4. Overlay of COMFA fields with 4. CoMFA contour plot (StDev*Coeff) of the steric and electrostatic components (contoured by contribution at 80% and 20%) of the CoMFA field based upon all 29 compounds using a 1 Å grid box. Regions where the model favors (green) or disfavors (yellow) steric bulk and favors (blue) or disfavors (red) positive charge are shown.

the structures of protein ligands and small molecule antagonists provide a useful basis for peptidomimetic design. This approach has played a role in the rational design of RGD-based inhibitors of the platelet integrin gpIIb/IIIa [26]. The results presented here suggest that a similar approach may prove fruitful in design of non-peptide Leu-Asp-Val analogs against VLA4.

Acknowledgements

We would like to Diane Leone and William Yang for generating the *in vitro* biological data, Paul Lyne, Claudio Chuaqui, Russ Petter and Laurie Castonguay

for useful suggestions, and Prashant Singh for his encouragement.

References

1. Leger, O.J., et al., Hum. Antibodies, **8** (1997) 3–16.
2. Molossi, S., et al., J. Clin. Invest., **95** (1995) 2601–2610.
3. Elices, M.J., Ciba Found. Symp., **189** (1995) 79–85.
4. Abraham, W.M., et al., J. Clin. Invest., **93** (1994) 776–787.
5. Sagara, H., et al., Int. Arch. Allergy Immunol., **112** (1997) 287–294.
6. Podolsky, D.K., et al., J. Clin. Invest., **92** (1993) 372–380.
7. Burkly, L.C., A. Jakubowski, and M. Hattori. Diabetes, **43** (1994) 529–534.
8. Yang, X.D., et al., Proc. Natl. Acad. Sci., **90** (1993) 10494–10498.

9. Chabot, S., G. Williams, and V.W. Yong, *J. Clin. Invest.*, **100** (1997) 604–612.
10. Seiffge, J. *Rheumatol.*, **23** (1997) 287–294.
11. Komoriya, A., et al., *J. Biol. Chem.*, **266** (1991) 15075–15079.
12. Humphries, M.J., et al., **189** (1995) 177–191.
13. Makarem, R., et al., *J. Biol. Chem.*, **269** (1994) 4005–4011.
14. Jones, E.Y., et al., *Nature*, **373** (1995) 539–544.
15. Wang, J.H., et al., *Proc. Natl. Acad. Sci. (USA)*, **92** (1995) 5714–5718.
16. Ling, L., et al., *Biochemistry*, **37** (1998) 8743–8753.
17. Kubinyi, H., *QSAR and 3D QSAR in drug design. Part 1: methodology*. Kluwer, Dordrecht, **2** (1997) 457–466.
18. Cramer, R.D., D.E. Patterson, and J.D. Bunce, *J. Am. Chem. Soc.*, **110** (1988) 5959–5967.
19. Lin, K.C., et al., *J. Med. Chem.*, **42** (1999) 920–934.
20. Cho, S.J. and A. Tropsha, *J. Med. Chem.*, **38** (1995) 1060–1066.
21. Lobb, R.R., et al., *Cell Adhes. Commun.*, **3** (1995) 385–397.
22. *Cambridge Crystallographic Database*: 12 Union Road, Cambridge CB2 1EZ, UK.
23. *MOPAC*, Quantum Chemistry Program Exchange: Creative Arts Building 181, Indiana University, Bloomington, Indiana 47405, USA.
24. Agarwal, A., et al., *J. Med. Chem.*, **36** (1993) 4006–4014.
25. Renz, M.E., et al., *J. Cell. Biol.*, **125** (1994) 1395–1406.
26. Ku, J. *Am. Chem. Soc.*, **2** (1993) 897.